MRS Communications (2019), 9, 381–389
© Materials Research Society, 2019
doi:10.1557/mrc.2019.11

MRS Communications

Research Letter

Elastomer-based MEMS optical interferometric transducers for highly sensitive surface stress sensing for biomolecular detection

Kazuhiro Takahashi, Department of Electrical and Electronic Information Engineering, Toyohashi University of Technology, 1-1 Hibarigaoka, Tempakucho, Toyohashi, Aichi 441-8580, Japan; JST PRESTO, Chiyoda, Tokyo 102-0076, Japan
Toshinori Fujie, JST PRESTO, Chiyoda, Tokyo 102-0076, Japan; School of Life Science and Technology, Tokyo Institute of Technology, B-50, 4259 Nagatsuta-cho, Midori-ku, Yokohama 226-8501, Japan; Waseda Institute for Advanced Study, Waseda University, Shinjuku-ku, Tokyo 162-8480, Japan
Reina Teramoto, Department of Electrical and Electronic Information Engineering, Toyohashi University of Technology, 1-1 Hibarigaoka, Tempakucho, Toyohashi, Aichi 441-8580, Japan
Isao Takahashi, Nobutaka Sato, and **Shinji Takeoka*,** Department of Life Science and Medical Bio-Science, Graduate School of Advanced Science and Engineering, Waseda University, Shinjuku-ku, Tokyo 162-8480, Japan
Kazuaki Sawada, Department of Electrical and Electronic Information Engineering, Toyohashi University of Technology, 1-1 Hibarigaoka, Tempakucho, Toyohashi, Aichi 441-8580, Japan

Address all correspondence to Kazuhiro Takahashi, Toshinori Fujie at **takahashi@ee.tut.ac.jp**; **t_fujie@bio.titech.ac.jp**

(Received 5 November 2018; accepted 14 January 2019)

Abstract

We developed a microelectromechanical-system optical interferometer based on an elastomer nanosheet using a polystyrene-polybutadiene-polystyrene (SBS) triblock copolymer for a suspended membrane as a way to improve the stress sensitivity for surface stress detection. The elastomeric SBS nanosheet provides a low Young's modulus of 28 ± 11 MPa, a large elastic strain of 24 ± 12%, and high adhesiveness, of which the surface charge and mechanical property are tunable by layer-by-layer (LbL) deposition of polysaccharides. A freestanding SBS nanosheet can be formed above a microcavity using a dry transfer technique without applying vacuum or high-temperature processes. The maximum deflection associated with molecular adsorption increased by sevenfold compared with a parylene-C-based optical interferometric transducer.

Introduction

A detection technique for various biomarkers in blood or urine enables us to make an at-home diagnosis simply, rapidly, and inexpensively. In particular, semiconductor-based biosensors such as ion-sensitive field-effect transistors (ISFETs) and microelectromechanical-system (MEMS)-based biosensors are expected to be developed for multi-marker detection using a single chip. ISFETs detect the charge of molecules immobilized on a channel for ion,[1,2] DNA,[3] or protein[4] detection. Although an ISFET-based biosensor can realize a large-scale integration for the parallel processing of multiple biomarkers, the detection area is limited by several nanometers from the substrate surface owing to the Debye length, and therefore an ISFET-based biosensor cannot be applied to the detection of charged macromolecules.[5] For the detection of biomacromolecules such as proteins, a MEMS-based biosensor that uses nanomechanical deflection caused by molecular binding to an antibody fixed on the sensing area is applied.[6] The static deformation is proportional to the surface stress caused by the Coulomb repulsive force between adsorbed molecules.[7] Based on the sensing method of the stress-induced nanomechanical deflection, MEMS surface stress sensors have been used for various targets such as DNA,[8] RNA,[9] proteins,[10] viruses,[11] and different chemicals.[12] Surface stress-based biosensors unconstrained by molecular size can possibly allow the establishment of multi-biomarker detection using different antibodies immobilized on individual sensor pixels. In addition, surface stress occurs not only with molecular adsorption but also with the structural changes to the biomacromolecules,[13,14] and therefore, a surface stress-based sensor can be used to conduct both quantitative and qualitative analyses of adsorbed molecules.

Conventional MEMS surface stress sensors have adopted capacitive[15] or piezoresistive[16,17] methods for an electrical readout transduced from the nanomechanical deflection. However, the limit of detection of the MEMS surface stress sensor is less than that of other biosensors.[18] To solve this problem, we recently developed a surface stress-based biosensor that uses a MEMS Fabry–Perot interferometer (FPI) with a silicon photodiode.[19] Using the drastic change in transmittance caused by membrane deformation of several

* This author was an editor of this journal during the review and decision stage. For the JMR policy on review and publication of manuscripts authored by editors, please refer to http://www.mrs.org/editor-manuscripts/.

https://doi.org/10.1557/mrc.2019.11 Published online by Cambridge University Press

tens of nanometers, the electrical readout signal is obtained as a photocurrent with a high signal-transducing efficiency. In addition, the proposed sensor can utilize the signal processing technique of a complementary metal–oxide–semiconductor image sensor.[20] The integrated FPI sensor array enabled us to develop a label-free multi-biosensing platform with high sensitivity.

In terms of the sensitivity of surface stress sensors, the suspended membrane of the FPI requires a soft material with a low Young's modulus, which offers improved sensitivity with molecular adsorption. Capacitive sensors and piezoresistive sensors use a semiconductor or metal for the deformable membrane because these materials allow a change in capacitance or resistance associated with membrane deformation for signal transduction, respectively. In contrast, optical interferometric sensors can accommodate organic materials for a deformable membrane. The previously fabricated FPI sensor used parylene-C with a Young's modulus of 2.8 GPa as the deformable membrane, and was shown to be able to detect antigens at a concentration of 10 ng/mL.[21] In this regard, an elastomer seems to be the most promising material for a stress sensor because of the low Young's modulus of 1–100 MPa, which is two to three orders of magnitude smaller than that of plastic materials, such as polymethylmethacrylate, polystyrene, and poly (*para*-xylylene) (parylene).

We previously developed an elastomer sheet hundreds of nanometers thick using a polystyrene-polybutadiene-polystyrene (SBS) triblock copolymer (referred to as an SBS nanosheet),[22] and demonstrated unique physical properties such as flexibility, stretchability, a low Young's modulus, and physical adhesiveness, reported in other types of nanosheets (e.g., polysaccharides).[23,24] In addition, the freestanding SBS nanosheet also achieves a large elastic deformation of 38% strain with cyclic straining.[25] Moreover, the freestanding SBS nanosheet can be attached to a substrate using a dry transfer technique without vacuum or high-temperature processes owing to the physical adhesiveness of the SBS nanosheet.[26]

In this paper, we propose an elastomer-based MEMS FPI transducer fabricated using the dry transfer of an elastomer nanosheet to cover the microcavities of a silicon substrate. We demonstrated a spectrum shift caused by nanomechanical deflection of the dry-transferred nanosheet in a liquid environment. The surface stress sensitivity of the FPI transducer associated with molecular adsorption was also evaluated using the surface-functionalized elastomer nanosheet.

Materials and methods

Materials

Polysaccharide electrolytes, chitosan (M_w 88,000), and sodium alginate (Na alginate, M_w 106,000) were purchased from Nacalai Tesque, Inc. (Kyoto, Japan) (see Supplementary Material Fig. S1). Polystyrene-*block*-polybutadiene-*block*-polystyrene (SBS; M_w 140,000) was purchased from Sigma-Aldrich Japan (Tokyo, Japan). Poly(vinylalcohol) (PVA, M_w 22,000, 86.5–89% hydrolyzed) was purchased from Kanto Chemical Co., Inc. (Tokyo, Japan). All organic solvents (reagent grade) were purchased from Kanto Chemical Co., Inc. (Tokyo, Japan) and used without purification. Silicon wafers (SiO_2 substrates) were purchased from KST World Co. (Fukui, Japan), and cut into an appropriate size (typically 2 cm × 2 cm), and immersed in a mixture of sulfuric-acid/hydrogen-peroxide (3/1 v/v) at 120 °C for 15 min before being extensively rinsed with deionized (DI) water (resistivity of 18 MΩ cm).

Preparation of SBS nanosheets and layer-by-layer deposition

Freestanding SBS nanosheets were prepared by following our previous report (see Supplementary Material Fig. S2).[22] In brief, a polyethylene terephthalate (PET) film was used as a base film. Next, an aqueous solution of PVA (20 mg/mL) was coated onto the PET film as a sacrificial layer using a microgravure coating method (gravure speed of 30 rpm, line speed of 1.3 m/min, drying temperature of 100 °C). Subsequently, the SBS polymer dissolved in tetrahydrofuran was coated onto the PVA/PET film (rotation speed of 30 rpm, line speed of 1.3 m/min, drying temperature of 80 °C).

Next, for electrostatic immobilization of the analytical molecules, 5.5-layer pairs of chitosan and sodium alginate were formed on the SBS layer using a spin-coating assisted layer-by-layer (LbL) method. First, the SBS/PVA/PET film was attached to a PDMS slab for spin coating after the surface was treated with plasma cleaner (30 mA, 1 min). Then, 1 mg/mL of chitosan and 1 mg/mL of Na alginate dissolved in 1% (v/v) acetic acid and DI water, respectively, were alternatively spin coated onto the SBS layer through a dual water-rinsing process (rotation speed of 4500 rpm, rotation time of 15 s for each spin-coating step). In the resulting film, the chitosan-layer-terminated LbL-SBS nanosheet was finally detached from the PET film using a paper-tape frame. After dissolving the sacrificial PVA layer in DI water, freestanding LbL-SBS nanosheets supported by the paper-tape frame were collected in air.

Atomic force microscopy (AFM) observation

The surface morphologies of the SBS and LbL-SBS nanosheets were analyzed using an atomic force microscope (AFM, Innova SPM, Bruker Co., Ltd., MA, USA), equipped with a piezoscanner (maximum scan size of 50 μm × 50 μm). Tapping mode tips (RTESPA-CP, Silicon AFM Probes, Bruker, USA) were used for the surface scanning, with a resonance frequency within the range of 290–330 kHz. The AFM tapping phase images were filtered and analyzed using NanoScope Analysis software (Bruker).

X-ray photoelectron spectroscopy (XPS) analysis

For a chemical analysis of the SBS and LbL-SBS nanosheets, XPS was carried out using a JPS-9010TR with a monochromatic Al KR x-ray source (1486.6 eV) incident at 90° relative to the axis of a hemispherical energy analyzer.

https://doi.org/10.1557/mrc.2019.11 Published online by Cambridge University Press

Photoelectrons were collected at a takeoff angle of 90° from the surface, and using an analyzer spot diameter of 1.1 mm. The survey spectra were collected from 0 to 1100 eV, and the high-resolution spectra were obtained for C1s, O1s, and N1s. All spectra were collected at room temperature with a base pressure of less than 1×10^{-8} Pa. Electron binding energies were calibrated with respect to the C1s line at 284 eV.

Bulge test

Mechanical properties of SBS and LbL-SBS nanosheets were evaluated by a bulge test. Ultimate tensile strength and elastic modulus of the nanosheets were determined using following equations:

$$\sigma = \frac{P \times a^2}{4 \times h \times d} \quad (1)$$

$$\varepsilon = \frac{2 \times d^2}{3 \times a^2} \quad (2)$$

$$E = \frac{\sigma}{\varepsilon} \quad (3)$$

where σ, P, a, h, d, ε, and E represent the tensile stress, applied pressure, radius of the circular hole of the steel plate, thickness, deflection, tensile strain, and elastic modulus of the thin film, respectively.

Characterization of LbL-SBS nanosheets

We obtained 5.5-layer pairs of chitosan/Na alginate on an SBS nanosheet using the LbL method. The thickness of the pristine SBS nanosheet was 477 ± 16 nm, whereas that of the LbL-SBS nanosheet was 493 ± 13 nm. Therefore, the subtracted thickness of the 5.5-LbL film was 16 ± 3 nm, which showed good agreement with a previous result.[23] The AFM surface morphology of the LbL-SBS nanosheet was relatively smooth, compared with that of the pristine SBS nanosheet (Fig. 1). Notably, the tapping-phase images reveal a phase-separated structure of the SBS nanosheet, which was hindered after the LbL deposition. Correspondingly, the surface roughness (R_q) of the LbL-SBS nanosheet (0.52 ± 0.0067 nm) became half that of the pristine SBS nanosheet (1.2 ± 0.060 nm), as shown in Table I. The LbL formation on the SBS nanosheet was also confirmed through an XPS analysis, which showed the presence of a new N1s peak at 400 eV (Fig. 2).

The mechanical influence of the LbL film on the SBS nanosheet was also evaluated using a bulge test (Fig. 3a). Both nanosheets were deflected by the applied air pressure in a step-

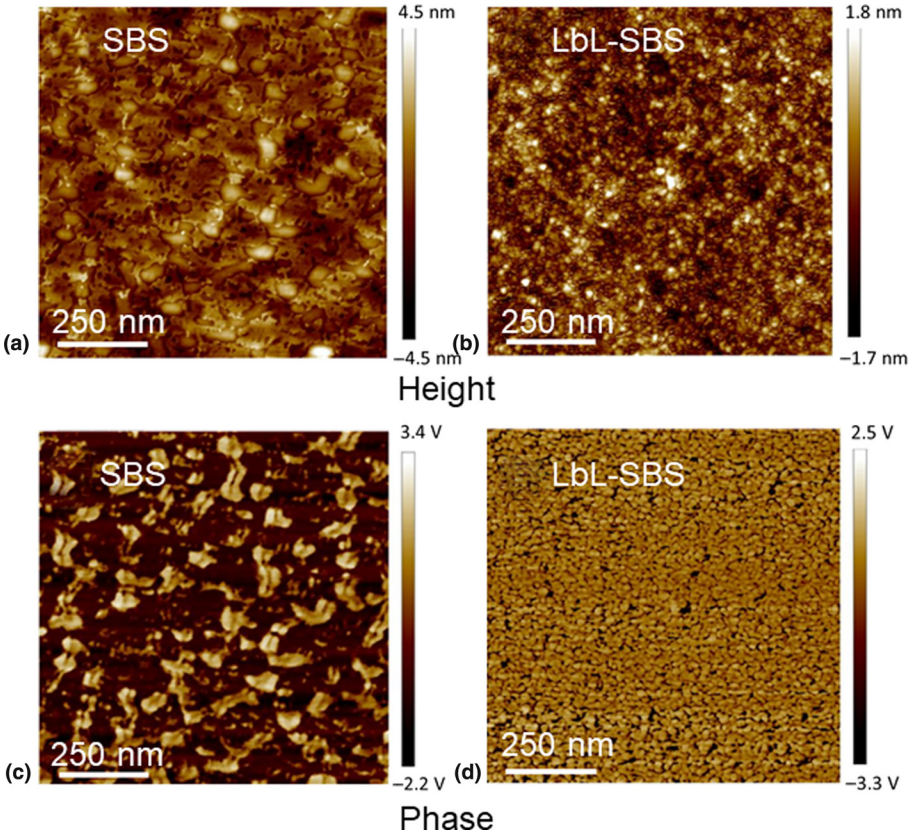


Figure 1. AFM characterization of LbL-SBS nanosheets. Top panels: height images of (a) SBS and (b) LbL-SBS. Bottom panels: phase images of (c) SBS and (d) LbL-SBS.

https://doi.org/10.1557/mrc.2019.11 Published online by Cambridge University Press

Table I. Surface roughness of SBS and LbL-SBS nanosheets

Sample	R_a (nm)	R_q (nm)
SBS ($n = 3$)	0.94 ± 0.052	1.2 ± 0.060
LbL-SBS ($n = 3$)	0.42 ± 0.0026	0.52 ± 0.0067

wise manner (Fig. 3b). According to the stress–strain curve based on the deflection, the elastic modulus of the LbL-SBS nanosheet (0.125 ± 0.033 GPa) was 4.5 times higher than that of the SBS nanosheet (0.028 ± 0.011 GPa) (Fig. 3c). Because the elastic modulus of the chitosan/Na alginate nanosheets was around 1 GPa,[23] the chitosan/Na alginate layer increased the elastic modulus of the LbL-SBS nanosheet. However, the elastic modulus of the LbL-SBS nanosheet was still 22.4 times smaller than that of a typical diaphragm, such as parylene-C [https://vsiparylene.com/parylene-advantages/properties/ (accessed September 25, 2018)].

Device design

Design of optical interferometric transducer

Figure 4(a) shows a schematic illustration of a MEMS optical interferometry-based surface stress transducer constructed using a suspended membrane over a silicon substrate with an air gap. The suspended membrane and the substrate act as two reflecting mirrors. An optical length configured by the air gap and the suspended membrane determines the optical interference. The target molecules are specifically bound using pre-immobilized receptors on the membrane such as an antigen–antibody reaction. The SBS nanosheet is utilized as the suspended membrane to increase the stress sensitivity owing to a low Young's modulus. When charged biomolecules are bound on the elastomer nanosheet, the membrane deforms into the upper direction by electrostatic repulsive force of the adsorbed molecules,[27] resulting in a redshift of the optical interference peak wavelength. To obtain an electrical signal, a photodetector can be implemented under the FPI for measuring the transmission light intensity. When a single wavelength light such as an LD or LED is illuminated onto the FPI, the intensity of the incident light on the photodetector is drastically changed. Therefore, we can obtain the electrical readout signal as a photocurrent. A drawback of a highly sensitive label-free biosensor is a trade-off relationship between the sensitivity and false positive responses, and the proposed surface stress sensor responds to temperature change, pressure change, etc. To avoid the false positive responses, a reference sensor without receptor molecules is required, resulting in discrimination with positive and false positive responses.

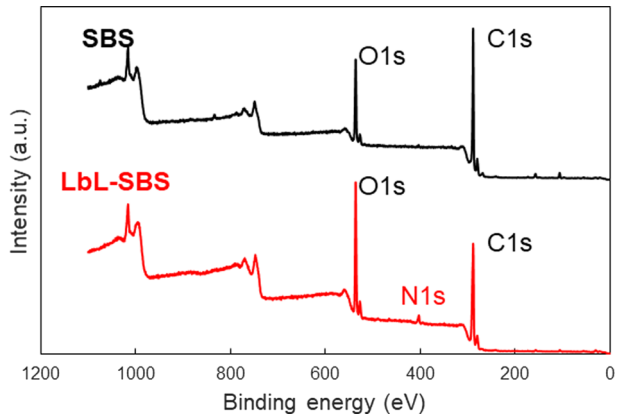


Figure 2. XPS spectra of SBS and LbL-SBS nanosheets. The N1s peak attributed to amine groups of chitosan was found for LbL-SBS.

Mechanical simulation

Compared to a previously reported surface stress transducer using a piezoresistive method, the proposed transducer used a soft material with a Young's modulus of 0.01–1 GPa, which is expected to improve the stress sensitivity. To estimate the sensitivity using an LbL-SBS nanosheet, a mechanical deflection of the suspended membrane associated with the surface stress was calculated by applying the finite element method (FEM) using COMSOL. The suspended membrane was designed to have a diameter of 50–500 μm and a thickness of 600 nm. The physical parameters of the LbL-SBS nanosheet were a Young's modulus of 125 MPa, Poison's ratio of 0.49, and density of 0.95 g/cm^3. Figure 4(b) shows the calculated deformation with isotropic compressive surface stress applied at the periphery of the membrane.[17] The result indicates that the LbL-SBS membrane with a diameter of 500 μm is deflected upward, reaching 947 nm with 1 mN/m. The typical deflection curve as a function of the surface stress is shown in Fig. 4(c). For quantitative comparison of transducers, we also calculated the deflection of a conventional cantilever type. The minimum detection limit of the surface stress of the conventional cantilever transducer have been reported to be 0.1–1 mN/m,[17] which agrees well with our calculation result with 500-μm-long, 100-μm-wide, and 1-μm-thick. With the minimum detectable displacement of 50 pm using the optical interferometry method,[28] the detection limit of the surface stress was obtained to be 0.1 μN/m or less, which is three orders of magnitude greater than a conventional surface stress transducer. From the point of view of the MEMS structure, the stiffness of the clamped membrane is much higher than that of a cantilever and bridge type. However, it is indicated that an elastomer nanosheet with an edge-clamped circular diaphragm decreases the total stiffness owing to the low Young's modulus and thin small thickness.

Fabrication

An elastomer-based MEMS FPI transducer was fabricated using an LbL-SBS nanosheet (see Supplementary material Fig. S3). Based on the mechanical simulation, we prepared LbL-SBS nanosheets for the device fabrication with the actual thickness of 560 nm. To form a suspended membrane with a microcavity structure, a Si wafer with shallow trenches was

https://doi.org/10.1557/mrc.2019.11 Published online by Cambridge University Press

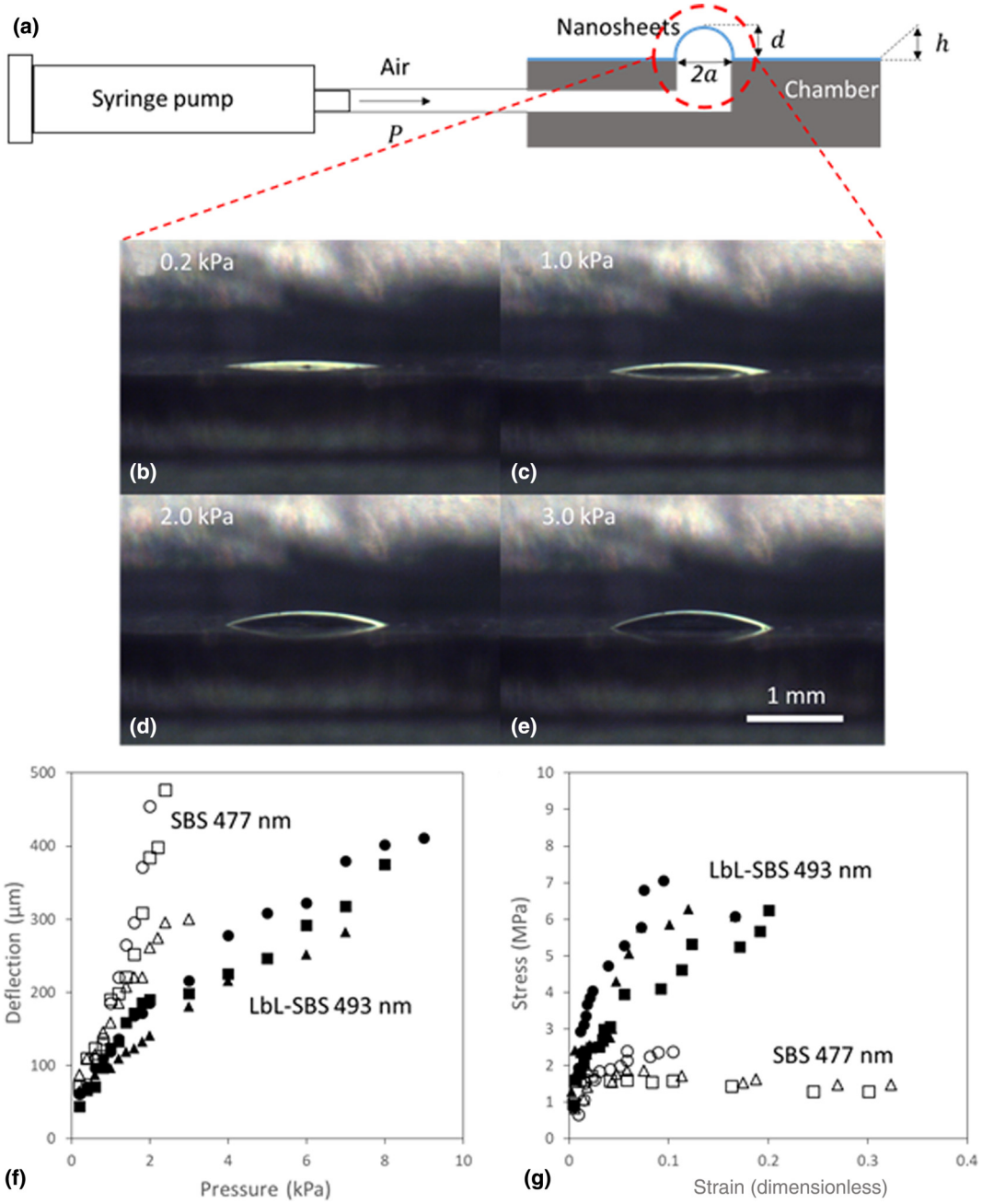


Figure 3. (a) Schematic representation of an apparatus for bulge test. (b–e) Cross-sectional images of deflected LbL-SBS nanosheets, sequentially compressed using external pressure of 0.2–3.0 kPa, respectively. (f) Pressure-deflection and (g) stress–strain curves of SBS nanosheets with thickness of 477 nm, and LbL-SBS nanosheets with thickness of 493 nm [i.e., $n = 3$ for SBS (blank symbol) and LbL-SBS (filled symbol), respectively].

prepared using reactive ion etching. For an improvement of the adhesion between the SBS nanosheet and Si substrate, a silane-coupling agent was coated onto the Si wafer, followed by a transferring of the nanosheet onto the Si wafer. An LbL-SBS nanosheet was developed on a PET film with a pre-laminated PVA sacrificial layer, as mentioned above. The LbL-SBS nanosheet was released from the PET film by dissolving the PVA layer in hot water at 60 °C. After drying, the released LbL-SBS nanosheet was transferred onto the Si substrate under dry conditions at room temperature. The high adhesiveness of the elastomer nanosheet provides permanent bonding without a vacuum process or high-temperature bonding.

Optical property

Figure 4(d) shows an optical microscope image of the developed freestanding LbL-SBS nanosheet with a diameter of 50

https://doi.org/10.1557/mrc.2019.11 Published online by Cambridge University Press

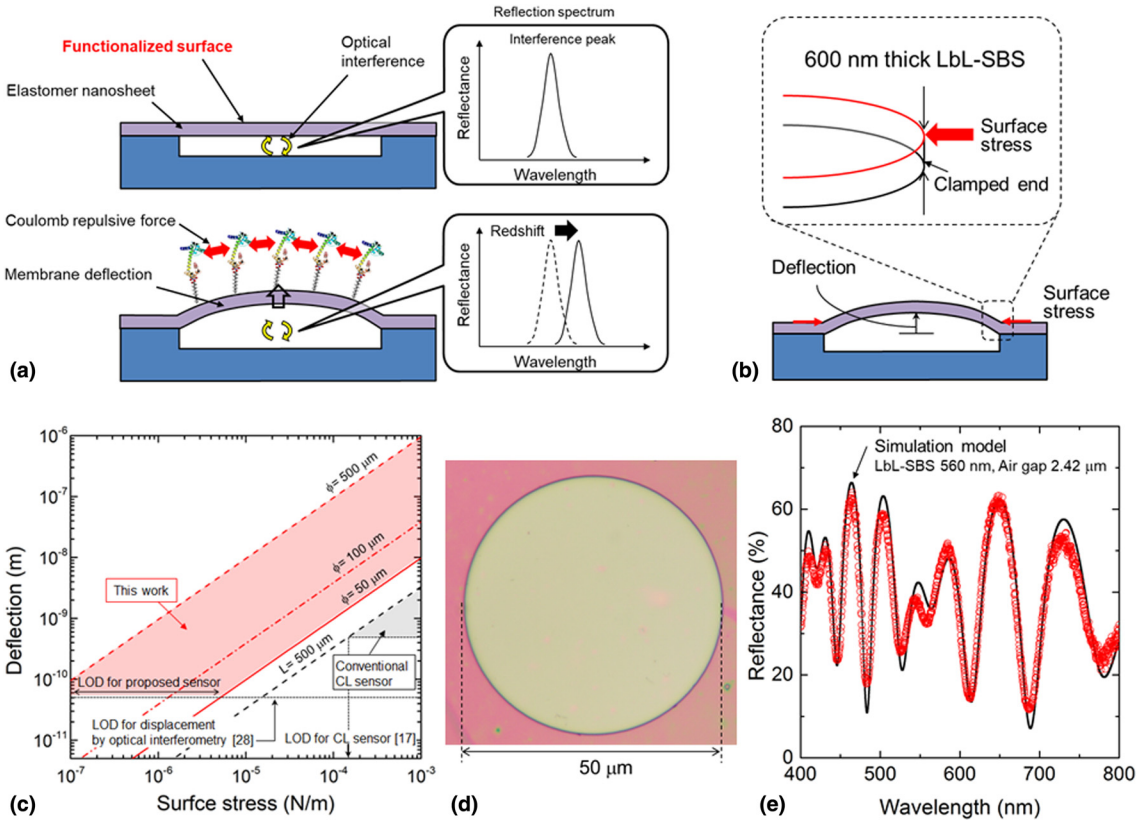


Figure 4. (a) Schematic image of the surface stress sensor based on a MEMS FPI. The FPI consists of a suspended thin film and an air gap, which determine the interference peaks of the reflection spectrum. The peak position is red shifted in association with the membrane deflection caused by Coulomb repulsive force adsorbed molecules on functionalized surface. (b) Mechanical deflection of elastomer nanosheet induced by surface stress simulated using FEM. The sensing membrane was designed to have a diameter of 50–500 μm and a thickness of 600 nm. (c) Typical membrane deflection as a function of the surface stress is plotted for comparing proposed transducer and conventional cantilever (CL) sensor. Limit of detection (LOD) of surface stress is improved by two to three orders of magnitude compared to the CL sensor. (d) Optical micrograph of the developed FPI surface stress sensor. (e) Typical reflection spectrum of the FPI with the dry-transferred LbL-SBS nanosheet. The suspended LbL-SBS nanosheet was 560-nm thick and 50 μm in diameter.

μm. The reflection spectrum of the elastomer-based FPI was measured using microscopic spectroscopy. A spectrometer (Ocean Optics, USB2000) was attached to a reflection microscope (Olympus, BX51) using an optical fiber with a core diameter of 100 μm. The magnification of the objective lens was 20×, and the measurement spot diameter was 5 μm. Figure 4(e) shows a typical reflection spectrum of the FPI with the dry-transferred LbL-SBS nanosheet. Eight interference peaks were observed in the reflection spectrum from the diaphragm within the visible region. A fitting curve using a refractive index of 1.5 with a thickness of 560 nm and a gap of 2.42 μm showed good agreement with the experimental value.

Experimental results of MEMS interferometer

Evaluation of membrane deflection in liquid

For an evaluation of the sensitivity of the proposed transducer, an anti-bovine serum albumin antibody (anti-BSA) was used as a model molecule for the driving force to deform the membrane because the surface stress sensor can obtain a deformation of the membrane owing to an adsorption of any molecule. We prepared phosphate buffer saline (PBS) (pH 7.4) for a negative control, and 10 μg/mL anti-BSA dissolved in PBS for the surface stress sensing. For comparison of the molecular adsorption capacity of a transducer surface, both transducers with Na alginate and chitosan coated on the top of the surface were prepared. Antibody molecules are expected to be adsorbed by the electrostatic interaction on the surface of the chitosan, whereas the molecular adsorption capacity of Na alginate surface is expected to be low. The reflection spectrum from the FPI transducer in the solution was measured using the same microscopy setup as mentioned above.

Figures 5(a) and 5(b) show typical reflection spectra of the FPI with a Na alginate surface and a chitosan surface in a PBS solution corresponding to the treatment time, respectively. All spectral shifts shown in Fig. 5 were recorded as moving picture (see Supplementary Video S1). The movie shows the spectral shift in the first 10 min of Fig. 5(a) at 50× speeds. The arrows in Fig. 5 indicate the position where a certain peak has shifted. Although the peak positions of the reflection spectra

https://doi.org/10.1557/mrc.2019.11 Published online by Cambridge University Press

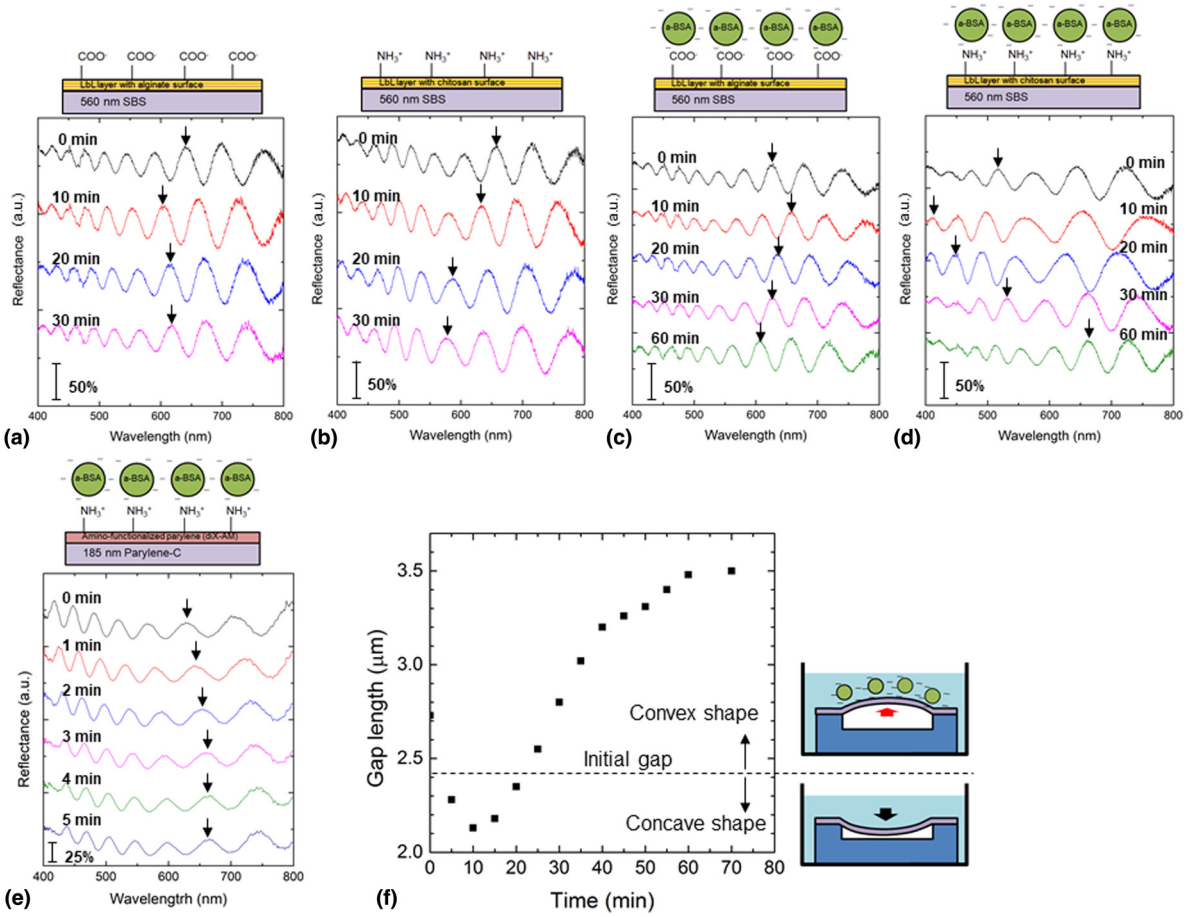


Figure 5. Spectrum shift of elastomer surface stress sensor by displacement of LbL-SBS nanosheet in a liquid. Typical reflection spectra of the FPI with (a) Na alginate surface and (b) chitosan surface in PBS solution corresponding to treatment time. Typical spectrum shift of the interferometric sensor with (c) Na alginate surface and (d) chitosan surface immersed in 10 μg/mL anti-BSA solution. (e) Typical spectrum shift of the parylene-C-based interferometric sensor immersed in a 10 μg/mL anti-BSA solution. (f) The time course of the membrane position is plotted. Although the shape of the membrane for the first 20 min showed a concave shape, the membrane position gradually increased and maintained a convex shape through the immobilization of antibody molecules.

were found to redshift immediately after being inserted into the PBS which is considered to be physical influence due to surface tension of PBS, the spectra of both devices were found to blue shift after 30 min of immersion in the PBS, indicating that the membrane was deformed into a lower direction. It is thought that air in the microcavity gradually leaked owing to the gas permeability of the elastomer nanosheet and no molecular adsorption on the membrane in PBS. In addition, the transient response of the membrane when the membrane comes in contact with the liquid can be relaxed by adding surfactants to reduce surface tension.

Figures 5(c) and 5(d) show typical spectrum shifts of the FPI transducer immersed in a 10 μg/mL anti-BSA solution. The transducer with the Na alginate surface behaved similarly as the spectral shift in PBS, whereas the FPI transducer with the chitosan surface demonstrated a redshift after observing the blueshift within the first 10 min. It should be noted that the motion of the spectral shift continued to redshift after changing from a blueshift. The elastomer membrane will deform into the upper direction in a liquid because the peak position has shifted toward the long wavelength side as compared with the initial state. The tenth order interference peak, indicated by an arrow, was found to move by 260 nm within 50 min. We assumed that the membrane was deformed by the surface stress induced through the molecular adsorption because the amino group of the chitosan layer can electrostatically adsorb the anti-BSA antibody. The difference in response between the chitosan and alginate surfaces can also be explained by the electrostatic interaction because anti-BSA with an isoelectric point of 4.8–5.2,[29] and a carboxyl group of alginate, are negatively charged whereas the amino-group of chitosan is positively charged at pH 7.4. Therefore, a freestanding elastomer membrane with a chitosan-functionalized surface using the LbL method demonstrated a surface stress response by adsorbing the anti-BSA antibody.

For a quantitative comparison, we measured the nanomechanical deflection using a previously developed parylene-C-based surface stress sensor with the same molecular concentration. The sensing membrane was formed using 20-nm thick

https://doi.org/10.1557/mrc.2019.11 Published online by Cambridge University Press

amino-functionalized parylene (diX-AM) and 185-nm thick parylene-C with a diameter of 50 μm. The tenth order interference peak was found to redshift by a maximum of 37 nm, and saturation in 5 min, as shown in Fig. 5(e). Despite the membrane thickness of parylene-based FPI, which is as thin as one-third of an LbL-SBS nanosheet, the SBS-based FPI exhibits an improvement of both the maximum deflection and the deflection speed owing to the elastic property of SBS.

The cavity length can be calculated through a rigorous coupled-wave analysis using experimentally obtained reflection spectra. Curve fitting was performed for the reflection spectra for 10 and 60 min treatment using the anti-BSA antibody PBS solution, which are the points furthermost to the left and right of spectrum peak shift (see Supplementary Material Fig. S4). A slight attenuation of the light intensity was found, whereas we obtained the agreed-upon fitting curves with interference peak positions. The membrane at 10 min moved down with 0.3 μm displacement compared to the initial gap length measured in air. Meanwhile, the gap length at 60 min was 3.48 μm, which means that the membrane deformed into the upper direction. From the calculation results, the time course of the membrane position was plotted, as shown in Fig. 5(f). The dotted line shows the initial flat state of the membrane. Whereas the shape of the membrane for the first 20 min concave, the membrane position gradually increased and maintained the convex shape through the immobilization of the molecules. This result suggests that the chitosan-functionalized membrane effectively adsorbed the biomolecules through an electrostatic interaction, resulting in a membrane deflection caused by a change in surface stress. In addition, the response of the membrane indicated the saturation of molecular adsorption to the freestanding membrane. Note, however, that the deformed membrane gradually changes back to the flat position, which is considered to be caused by pressure reduction due to air leakage. To measure concentration of target molecule, it is possible to evaluate by comparing the initial velocity of deflection response after adding an analyte. It is expected that highly sensitive surface stress sensing is associated with the molecular adsorption owing to the use of an elastomer nanosheet.

Conclusions

We developed an elastomer-based MEMS FPI using a dry transfer technique to form a microcavity. The fabricated FPI comprises a freestanding LbL-SBS nanosheet with a thickness of 560 nm provided a sufficient optical property such as reflectance and peak-to-valley ratio for optical biosensing. For molecular immobilization on the proposed transducer, a chitosan-functionalized elastomer nanosheet was used for the suspended membrane. We demonstrated the spectrum shift associated with the nanomechanical deflection of the dry-transferred freestanding LbL-SBS nanosheet in a liquid environment. The nanomechanical deflection caused by molecular adsorption was enhanced using an elastomer nanosheet for the deformable membrane, which enables the detection of biomarkers with high sensitivity by freely modifying the membrane surface, leading to a universal biosensing platform. The detection capability of the surface stress biosensor depends on the sensitivity of the transducer as well as the bio-interface such as the density of a cross linker and affinity of a receptor molecule. The elastomer transducer with improved surface stress sensitivity is expected to detect lower concentration of target molecules by optimization of the bio-interface on the elastomer transducer.

Supplementary material

The supplementary material for this article can be found at https://doi.org/10.1557/mrc.2019.11

Acknowledgments

This work was supported in part by a Grant-in-Aid for Young Scientists (A) (26709025), Grant-in-Aid for Scientific Research (B) (18H03539), and Grant-in-Aid for Scientific Research on Innovative Areas (18H05469) from the Japan Society for the Promotion of Science, and by the Precursory Research for Embryonic Science and Technology (PRESTO) (JPMJPR1526 and JPMJPR152A) from the Japan Science and Technology Agency.

References

1. M. Esashi and T. Matsuo: Integrated micro multi ion sensor using field effect of semiconductor. *IEEE Trans. Biomed. Eng. BME* **25**, 184 (1978).
2. K. Sawada, S. Mimura, K. Tomita, T. Nakanishi, H. Tanabe, M. Ishida, and T. Ando: Novel CCD-based pH imaging sensor. *IEEE Trans. Electron Devices* **46**, 1846 (1999).
3. T. Sakata, M. Kamahori, and Y. Miyahara: Immobilization of oligonucleotide probes on Si_3N_4 surface and its application to genetic field effect transistor. *Mater. Sci. Eng. C* **24**, 827 (2004).
4. Y. Ohno, K. Maehashi, K. Inoue, and K. Matsumoto: Label-free aptamer-based immunoglobulin sensors using graphene field-effect transistor. *Jpn. J. Appl. Phys.* **50**, 070120 (2011).
5. T. Sakata and Y. Miyahara: Direct transduction of allele-specific primer extension into electrical signal using genetic field effect transistor. *Biosens. Bioelectron.* **22**, 1311 (2007).
6. D. A. Raorane, M. D. Lim, F. F. Chen, C. S. Craik, and A. Majumdar: Quantitative and label-free technique for measuring protease activity and inhibition using a microfluidic cantilever array. *Nano Lett.* **8**, 2968 (2008).
7. M. Watari, J. Galbraith, H.-P. Lang, M. Sousa, M. Hegner, C. Gerber, M. A. Horton, and R. A. McKendry: Investigating the molecular mechanisms of in-plane mechanochemistry on cantilever arrays. *J. Am. Chem. Soc.* **129**, 601 (2007).
8. J. Fritz, M. K. Baller, H. P. Lang, H. Rothuizen, P. Vettiger, E. Meyer, H. J. Guntherodt, C. Gerber, and J. K. Gimzewski: Translating biomolecular recognition into nanomechanics. *Science* **288**, 316 (2000).
9. J. Zhang, H. P. Lang, F. Huber, A. Bietsch, W. Grange, U. Certa, R. McKendry, H.-J. Guntherodt, M. Hegner, and C. Gerber: Rapid and label-free nanomechanical detection of biomarker transcripts in human RNA. *Nat. Nanotechnol.* **1**, 214 (2006).
10. G. H. Wu, R. H. Datar, K. M. Hansen, T. Thundat, R. J. Cote, and A. Majumdar: Bioassay of prostate-specific antigen (PSA) using microcantilevers. *Nat. Biotechnol.* **19**, 856 (2001).
11. P. V. Gorelkin, A. S. Erofeev, G. A. Kiselev, D. V. Kolesov, E. V. Dubrovin, and I. V. Yaminsky: Synthetic sialylglycopolymer receptor for virus detection using cantilever-based sensors. *Analyst* **140**, 6131 (2015).

https://doi.org/10.1557/mrc.2019.11 Published online by Cambridge University Press

12. R. Berger, E. Delamarche, H. P. Lang, C. Gerber, J. K. Gimzewski, E. Meyer, and H. J. Guntherodt: Surface stress in the self-assembly of alkanethiols on gold. *Science* **276**, 2021 (1997).
13. M. K. Ghatkesar, H. P. Lang, C. Gerber, M. Hegner, and T. Braun: Comprehensive characterization of molecular interactions based on nanomechanics. *PLoS One* **3**, e3610 (2008).
14. K. Buchapudi, X. Xu, Y. Ataian, H.-F. Ji, and M. Schulte: Micromechanical measurement of AChBP binding for label-free drug discovery. *Analyst* **137**, 263 (2012).
15. S. Satyanarayana, D. T. McCormick, and A. Majumdar: Parylene micro membrane capacitive sensor array for chemical and biological sensing. *Sens. Actuators, B* **115**, 494 (2006).
16. K. W. Wee, G. Y. Kang, J. Park, J. Y. Kang, D. S. Yoon, J. H. Park, and T. S. Kim: Novel electrical detection of label-free disease marker proteins using piezoresistive self-sensing micro-cantilever. *Biosens. Bioelectron.* **20**, 1932 (2005).
17. G. Yoshikawa, T. Akiyama, S. Gautsch, P. Vettiger, and H. Rohrer: Nanomechanical membrane-type surface stress sensor. *Nano Lett.* **11**, 1044 (2011).
18. J. L. Arlett, E. B. Myers, and M. L. Roukes: Comparative advantages of mechanical biosensors. *Nat. Nanotechnol.* **6**, 203 (2011).
19. K. Takahashi, H. Oyama, N. Misawa, K. Okumura, M. Ishida, and K. Sawada: Surface stress sensor using MEMS-based Fabry–Perot interferometer for label-free biosensing. *Sens. Actuators, B* **188**, 393 (2013).
20. S. Maruyama, T. Hizawa, K. Takahashi, and K. Sawada: Optical-interferometry-based CMOS-MEMS sensor transduced by stress induced nanomechanical deflection. *Sensors* **18**(1), 138 (2018).
21. T. Takahashi, T. Hizawa, N. Misawa, M. Taki, K. Sawada, and K. Takahashi: Surface stress sensor based on MEMS Fabry–Perot interferometer with high wavelength selectivity for label-free biosensing. *J. Micromech. Microeng.* **28**, 054002 (2018).
22. N. Sato, A. Murata, T. Fujie, and S. Takeoka: Stretchable, adhesive and ultra-conformable elastomer thin films. *Soft Matter* **12**, 9202 (2016).
23. T. Fujie, N. Matsutani, M. Kinoshita, Y. Okamura, A. Saito, and S. Takeoka: Adhesive, flexible, and robust polysaccharide nanosheets integrated for tissue-defect repair. *Adv. Funct. Mater.* **19**, 2560 (2009).
24. T. Fujie: Development of free-standing polymer nanosheets for advanced medical and health-care applications. *Polym. J.* **48**, 773 (2016).
25. H. Kumagai, N. Sato, S. Takeoka, K. Sawada, T. Fujie, and K. Takahashi: Optomechanical characterization of freestanding stretchable nanosheet based on polystyrene-polybutadiene-polystyrene copolymer. *Appl. Phys. Express* **10**, 011601 (2017).
26. K. Takahashi, T. Fujie, N. Sato, S. Takeoka, and K. Sawada: MEMS optical interferometry-based pressure sensor using elastomer nanosheet developed by dry transfer technique. *Jpn. J. Appl. Phys.* **57**, 010302 (2018).
27. J. Fritz: Cantilever biosensors. *Analyst* **133**, 855 (2008).
28. M. Schmidt, B. Werther, N. Furstenau, M. Matthias, and T. Melz: Fiber-optic extrinsic Fabry–Perot interferometer strain sensor with <50 pm displacement resolution using three-wavelength digital phase demodulation. *Opt. Express* **8**, 475 (2001).
29. S. Ge, K. Kojio, A. Takahara, and T. Kajiyama: Bovine serum albumin adsorption onto immobilized organotrichlorosilane surface: Influence of the phase separation on protein adsorption patterns. *J. Biomater. Sci. Polym. Ed.* **9**, 131 (1998).

https://doi.org/10.1557/mrc.2019.11 Published online by Cambridge University Press